# Ricker-compliant deconvolution

*Jon Claerbout and Antoine Guitton*

## ABSTRACT

Ricker compliant deconvolution spikes at the center lobe of the Ricker wavelet. It enables deconvolution to preserve and enhance seismogram polarities. Expressing the phase spectrum as a function of lag, it works by suppressing the phase at small lags. A byproduct of this decon is a pseudo-unitary (very clean) debubble filter where bubbles are lifted off the data while onset waveforms (usually Ricker) are untouched.

## INTRODUCTION

A long-standing assumption in reflection seismology is that seismic sources are minimum phase (Robinson and Treitel, 1964). This means the source wavelet and its inverse (the decon filter) are both causal. The decon filter is derived from the data spectrum. Its inverse should be the source wavelet. These assumptions lead to the non-plausible source waveforms in Figure 1. We should be seeing something closer to the symmetrical Ricker wavelet (Ricker, 1953): let $Z = e^{i\omega dt}$ where $dt$ is the two way travel time from the gun (or the receiver) to the surface and back. Since the surface reflection coefficient is -1, the frequency response at the gun is $1 - Z$ and at the hydrophone is also $1 - Z$ making the composite response $1 - 2Z + Z^2$. Therefore, the Ricker wavelet results from a water-surface ghost at the marine gun convolved with another at the hydrophone (Lindsey, 1960). In all four of the deep-marine regions we tested and show in Figure 1, the minimum-phase source wavelets estimated with the Kolmogoroff method (see below) have the expected three lobes, but they are not symmetric. The first lobe is more than double the third. This is a long-standing issue in seismic processing (Levy and Oldenburg, 1982) and many methods based, for instance, on homomorphic transformations (Jin and Rogers, 1983), frequency domain filtering (Ghosh, 2000), higher order statistics (Sacchi and Ulrych, 2000) or stochastic methods (Velis, 2008) have been proposed to handle non minimum-phase wavelets.

In the conflict between the Ricker idea and the minimum-phase idea we take it here that the Ricker idea is closer to the truth (Rice, 1962). The main contribution of this paper is a method for finding phase that respects Ricker symmetry. The new time origin is at the center of the Ricker wavelet. With the new seismic wavelet, seismogram polarity will be seen more apparent. A byproduct of this approach is a debubble process giving results of outstanding clarity.

Our proposed method is a simple addition to the Kolmogoroff method in the lag-log domain (also known as the "cepstrum"). Parameterizing the logarithm of the

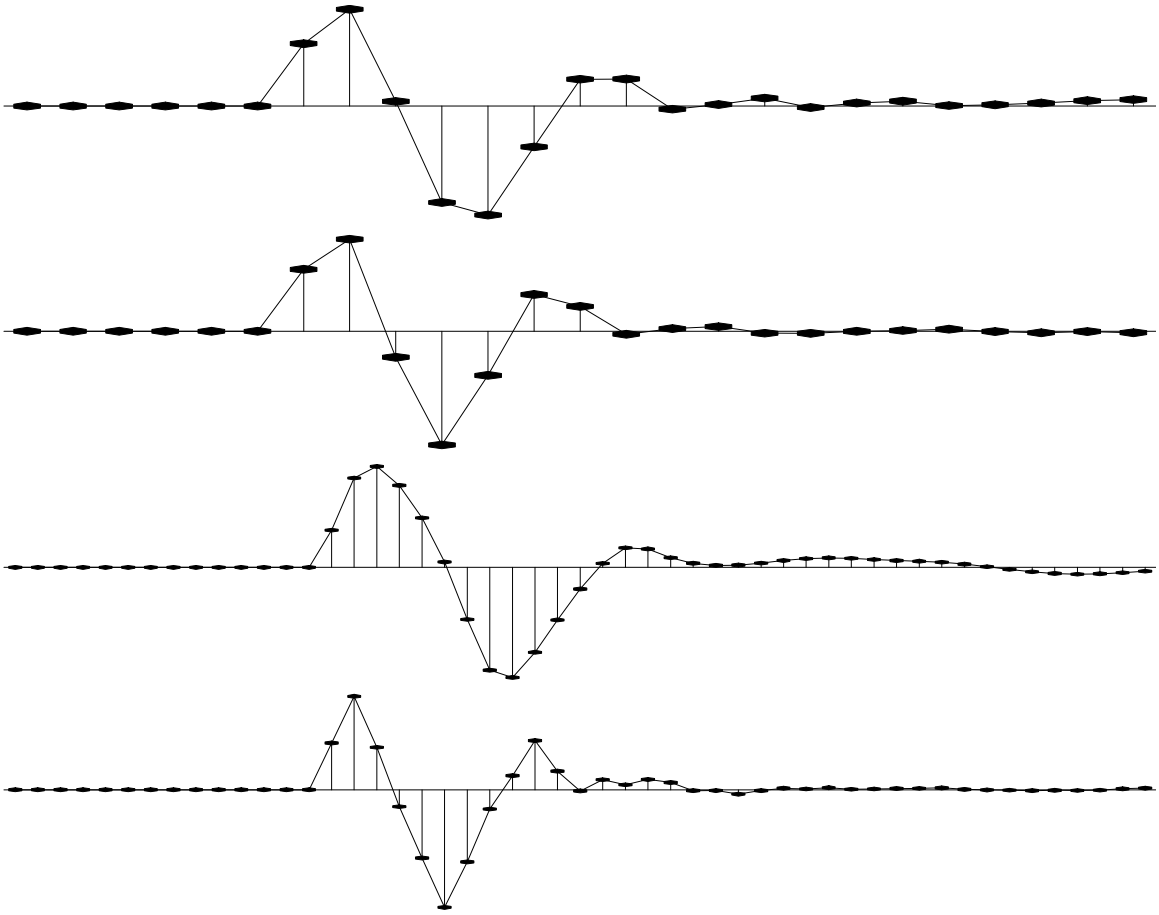

Figure 1: Estimated shot wavelets from four deep-marine regions when the minimum-phase assumption is made. They are not time symmetric about the middle lobe. Top two wavelets are from 4 ms data and the bottom two from 2 ms data. These results are based on data corrected for divergence. Spectra were averaged over many hundreds of inner-offset seismograms. These spectra were not smoothed. [**NR**]

spectrum in the time domain lays out parameter choices in a natural way along the "quefrency" axis. Wavelets presented here and computed in $N \log_2 N$ time from field data examples show the expected Ricker shape. We regard them as a final analytical stage before invoking iterative inverse theory for the wavelet estimation problem.

## BASICS OF LAG-LOG SPACE

Let $F(\omega)$ be a filter in frequency domain. Let $\ln F(\omega) = U(\omega)$ so the filter is $F(\omega) = e^{U(\omega)}$. With the definition $Z = e^{i\omega\Delta t}$ Fourier transforms become polynomials ($Z$-transforms). Thus $U(\omega)$ relates to the time function $u_\tau$ by a Fourier sum $U(\omega) = \sum_{\tau=0}^{\tau_{\max}} u_\tau Z^\tau$. The $u_\tau$ values will be our parameterization of the filter. Historically, the $\tau$ axis is called the "quefrency" axis though we sometimes refer to it as the "lag-log" axis.

The property of exponentials that $e^{A+B+C} = e^A\, e^B\, e^C$ has an interesting meaning when we exponentiate a $Z$-transform $\exp(A + B + C) = \exp(\sum_{\tau=1}^{\tau_{\max}} u_\tau Z^\tau)$. The $Z$-transform sum may be split up into small lags, medium lags, and large lags. This decomposes a filter (or waveform) into a sequence of three filters, each with its own meaning where for example in common marine seismology:

$$e^{A+B+C} = e^A\, e^B\, e^C \tag{1}$$

$$e^{\sum_{\tau=1}^{\tau_{\max}} u_\tau Z^\tau} = e^{\sum_1^c}\, e^{\sum_{c+1}^r}\, e^{\sum_{r+1}^{\tau_{\max}}} \tag{2}$$

$$\text{(wavelet)} = \text{(continuity)(Ricker)(bubble)} \tag{3}$$

where $c$ and $r$ define the boundaries of the continuity and Ricker regions, respectively. Equation (2) defines the boundaries of the three regions abruptly although in practice we blend them smoothly with sine-squared weighting. Changing the sign of $(A+B+C)$ changes a filter to its inverse. Both are parameterized by the same $A$, $B$, and $C$.

### Exploring $e^A$: band limiting filter

Theoretically, the output of a prediction-error filter tends to be white. In practice, energy near the Nyquist frequency will be nearly all noise, so nobody wants to see a white output. For this reason deconvolution is generally followed by band-pass filtering. Equation 2 integrates the two processes, deconvolution and the band pass. The parameter $c$ is analogous to the bandpass cutoff frequency, but it is a cutoff in lag hence resembles inverse frequency. Although we may hope to resolve some very short lags, we do not want our deconvolved data dominated by short lags. We have made no attempt to achieve a sharp cutoff, instead using a sine squared taper. Typically, we experiment with $c$ and have taken $c$ to correspond to about 7ms.

## Exploring $e^C$: debubbling filter

We may specify $u_\tau$ from prior knowledge, or from knowledge gained from various kinds of data averaging, or from some mixture of the two. Commonly we begin from Kolmogoroff spectral factorization (next section) giving us all the $u_\tau$. We may design a filter $e^{A+B+C}$ by over-riding Kolmogoroff with $A = 0$ and $B = 0$. Such a filter would do nothing to its inputs at small and intermediate lags but would affect longer lags. To see what happens, consider the filter $e^C = 1 + C + C^2/2! + \cdots \approx 1 + C$. Examine its leading coefficients. They are $(1, 0, 0, \cdots, 0, u_{r+1}, u_{r+2}, u_{r+3}, \cdots)$. Figure 2 shows the application of such a filter with $r = 15$. This operation on the data is called "debubbling". Debubbling in this manner seems to leave first arrivals untouched. The 15 interval gap on 4 ms data is 60 ms, a number half way between the "end of the ghosts" and the "onset of the bubbles". This result may be described as "textbook quality" (meaning it is the best we have ever produced).

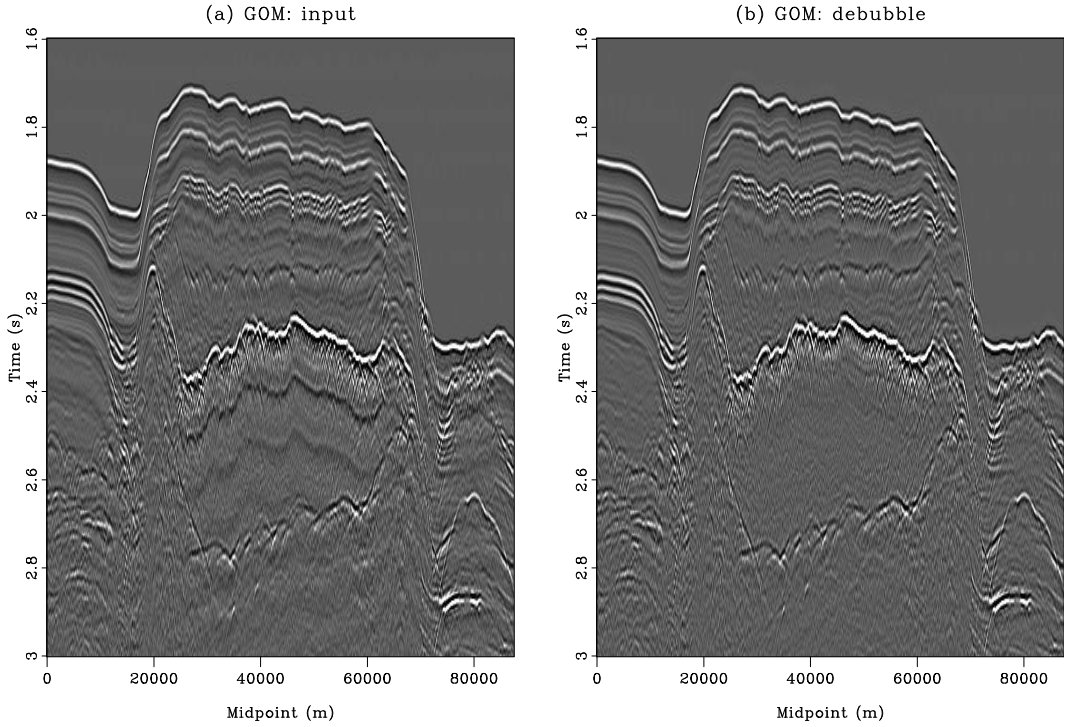


Figure 2: Gulf of Mexico data before (a) and after debubble (b). This process preserves the wave onset while it lifts off the bubbles. Here the effect of the process is visible nearly everywhere after 2.4 sec, but also visible around 1.85 sec. On blinking displays it is easy to see bubble removed nearly everywhere. [**NR**]

Before we go on to attack the middle-lag terms we review the starting point, Kolmogoroff spectral factorization.

## Kolmogoroff spectral factorization

When a time function such as $b_t$ vanishes at all negative time lags it is said to be causal. Its $Z$ transform is $B(Z) = b_0 + b_1 Z + b_2 Z^2 + b_3 Z^3 + \cdots$. Observe that $B(Z)^2$ is also causal because it has no negative powers of $Z$, alternately, because the convolution of a causal with a causal is causal. Likewise $e^B$ is causal because it is a sum of causals.

$$e^B \quad = \quad 1 + B + B^2/2! + B^3/3! + \cdots \tag{4}$$

Happily, this infinite series always converges because of the strong influence of the denominator factorials. The time-domain coefficients for $e^B$ could be computed the hard way, putting polynomials into power series, or $e^B$ may be computed by Fourier transforms. To do so, we would evaluate $B(Z)$ for many real $\omega$, and then invoke an inverse Fourier transform program to uncover the time-domain coefficients.

Let $r = r(\omega)$, $\phi = \phi(\omega)$, and $Z^\tau = e^{i\omega\tau}$. Let us investigate the consequence of exponentiating a causal filter.

$$|r|e^{i\phi} \quad = \quad e^{\ln|r| + i\phi} \quad = \quad e^{\sum_\tau b_\tau Z^\tau} \tag{5}$$

Notice a pair of filters, both causal and inverse to each other.

$$|r|e^{i\phi} \quad = \quad e^{+\sum_\tau b_\tau Z^\tau} \tag{6}$$

$$|r|^{-1}e^{-i\phi} \quad = \quad e^{-\sum_\tau b_\tau Z^\tau} \tag{7}$$

A filter from any such pair is said to be "minimum phase". Many filters are not minimum phase because they have no causal inverse. For example the delay filter $Z$. It's inverse, $Z^{-1}$ is not causal. Such filters do not relate to a causal complex logarithm. If they have a logarithm, it must be non causal.

Given a spectrum $r(\omega)$ we can construct a minimum-phase filter with that spectrum. Since $r(\omega)$ is a real even function of $\omega$, the same may be said of its logarithm. Let the inverse Fourier transform of $\ln|r(\omega)|$ be $e_\tau$, where $e_\tau$ is a real even function of time. Imagine a real odd function of time $o_\tau$.

$$|r|e^{i\phi} \quad = \quad e^{\ln|r| + i\phi} \quad = \quad e^{\sum_\tau (e_\tau + o_\tau) Z^\tau} \tag{8}$$

The phase $\phi(\omega)$ transforms to $o_\tau$. We can assert causality by choosing $o_\tau$ so that $e_\tau + o_\tau = 0$ for all negative $\tau$. This defines $o_\tau$ at negative $\tau$. Since $o_\tau$ is odd, we also know its values at positive lags. This creates a causal exponent which creates a causal minimum-phase filter with the specified spectrum. Therefore the causal minimum-phase filter is simply obtained by multiplying $e_\tau$ by a step function of height 2 to preserve the real part. This computation is called Kolmogoroff spectral factoring. The word "factoring" enters because in applications one begins with an energy spectrum $|r|^2$ and factors it into an $re^{i\phi}$ times its conjugate (time reverse).

## Ricker compliant decon

Start with the $b_\tau$ resulting from a Kolmogoroff factorization described above. Split it into even and odd parts, $u_\tau^{\text{odd}} = (b_\tau - b_{-\tau})/2$ and $u_\tau^{\text{even}} = (b_\tau + b_{-\tau})/2$ whose sum is $b_\tau$. The even part Fourier transforms to the logarithm of the amplitude spectrum (i.e., equation 8). The odd part Fourier transforms to the phase spectrum. Here we monkey with the phase while not changing the amplitude. We simply taper $u_\tau^{\text{odd}}$ towards zero for small lags. Figure 3a shows an illustration of an odd function together with the weighting function going smoothly to zero at negative lags in Figure 3b. The parameter $\tau_a$ controls the amount of anticausality in the wavelet. Figure 4 examines the consequences of various numerical choices of $\tau_a$ for the data in Figure 2a. In practice, the cepstrum of all traces is averaged before applying the decon. As we increase the anticausality, the time function of the wavelet $e^B$ increases in symmetry near $t = 0$. Our favored choice is $\tau_a = 64$ ms: it is larger than the Ricker width, about 20 ms, but not as large as the bubble delay, about 150 ms.

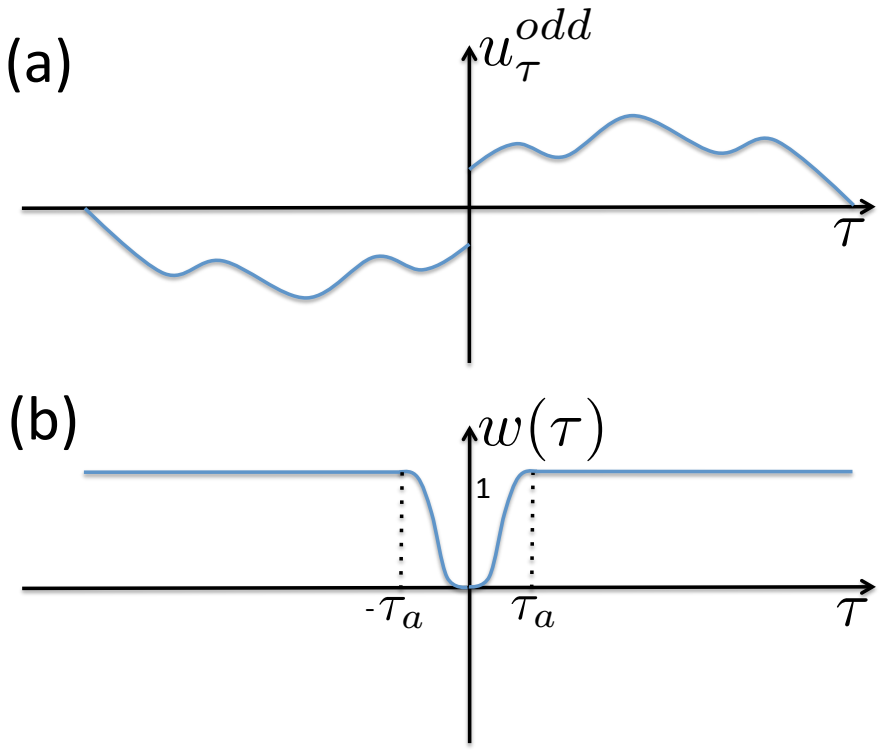


Figure 3: The odd part of $b_\tau$ (a) and the weighting function (b). The parameter $\tau_a$ determines the amount of anticausality in the wavelet. [**NR**]

Removing all the phase of any wavelet makes it symmetric in time. Any deconvolution filter can be made Ricker-compliant simply by transforming its phase function

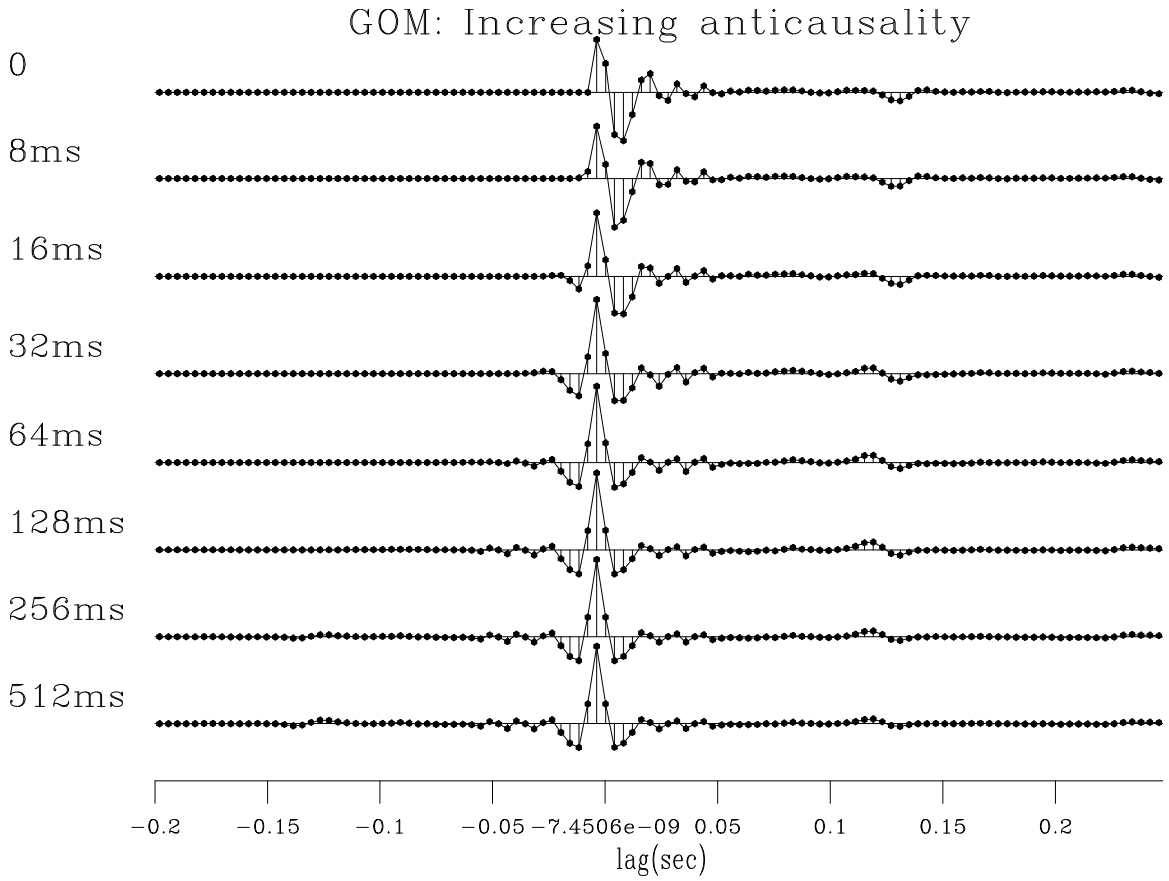


Figure 4: Gulf of Mexico $\Delta t = 4$ ms: Increasing the anticausality $\tau_a$ in Ricker compliant decon. Too much ($\tau_a > 128$ ms) causes half the bubble to appear before the shot. $\tau_a = 0$ ms corresponds to the minimum-phase wavelet. In this manuscript, our favored choice is $\tau_a = 64$ ms. [**NR**]

from frequency to time lag. Suppressing the phase only near zero lag makes the wavelet symmetric only near zero lag (Ricker like).

The next section presents Ricker deconvolutions and debubbling examples on three field datasets. For all these examples, we use portions of the near-offset sections compensated for spherical divergence and attenuation (applying a $t^2$ correction). All these results demonstrate the effectiveness of the proposed method for estimating Ricker-like, zero-phase wavelets as well as debubbling seismic data.

## RICKER DECONVOLUTION AND DEBUBBLING RESULTS

We first start by presenting results of the debubbling process on a dataset from offshore Baja California (also called "Cabo" in this manuscript) shown in Figure 5a. Debubbling (Figure 5b) is very effective as the bubbles are lifted off everywhere in the section (the first bubble arrives 150 ms after the main spike.)

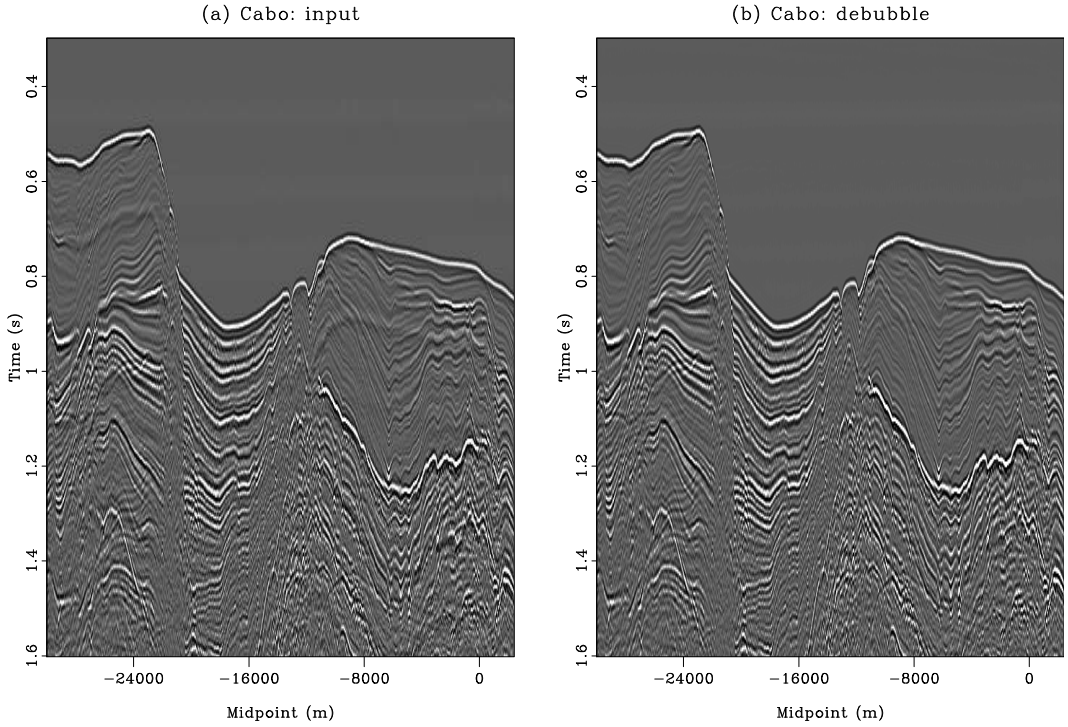


Figure 5: Cabo data before (a) and after debubble (b). This process preserves the wave onset while it lifts off the bubbles. [**NR**]

Then, the Ricker deconvolution applied to the Gulf of Mexico dataset of Figure 2b is shown in Figure 6a with $c = 0$ ms and in Figure 6b with $c = 10$ ms. Increasing $c$ acts as a bandpass filter by attenuating high-frequencies. The same filtering effect is seen with the Cabo dataset in Figure 7b. Notice in both Figures 6 and 7 how the deconvolution is able to remove the Ricker-like behavior of the main reflections.

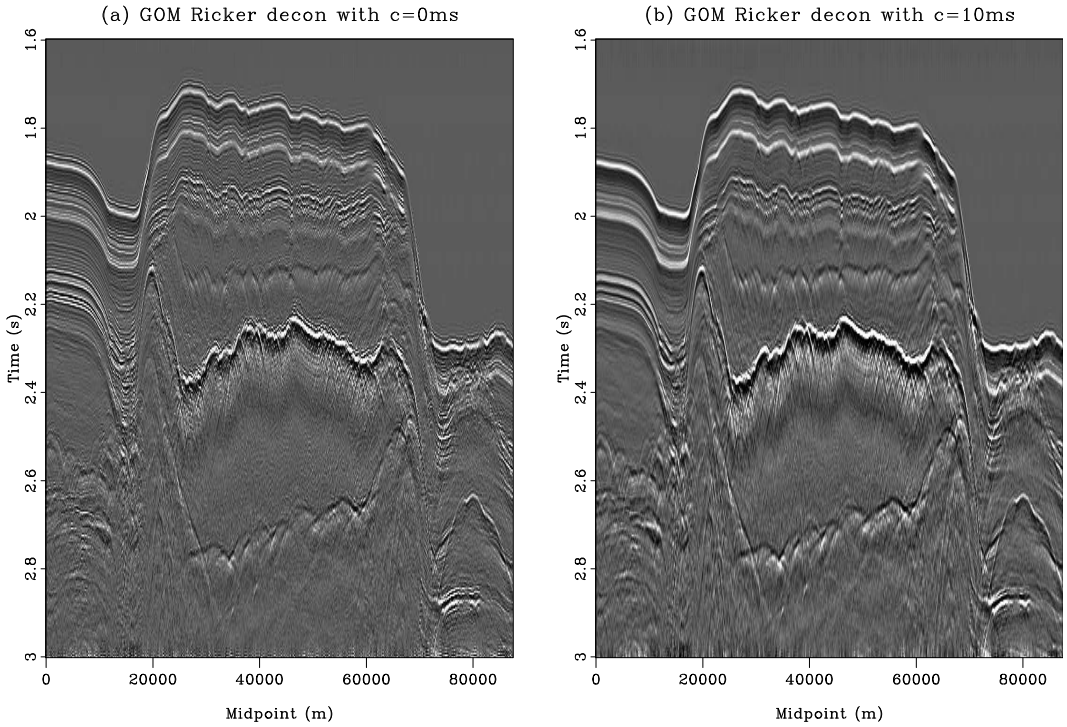


Figure 6: Ricker deconvolution results applied to the Gulf of Mexico dataset in Figure 2 for (a) $c = 0$ ms and (b) $c = 10$ ms. [**NR**]

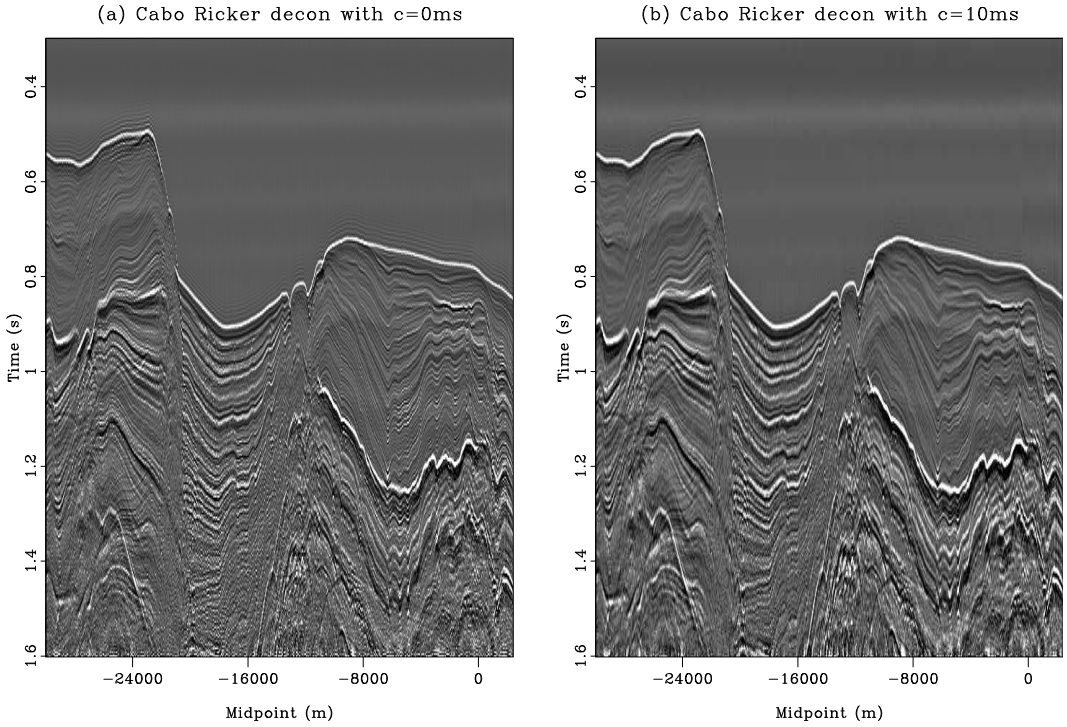


Figure 7: Ricker deconvolution results applied to the Cabo dataset for (a) $c = 0$ ms and (b) $c = 10$ ms. [**NR**]

Figure 8 displays the different waveforms extracted from the Gulf of Mexico and Baja California datasets. Figures 8a and 8b show the Ricker wavelets (including the bubbles) extracted with our process. Figures 8c and 8d show the bubbles only ($e^C$ in equation 2). The bubbles, deconvolved from the ghosts, show uniform polarity.

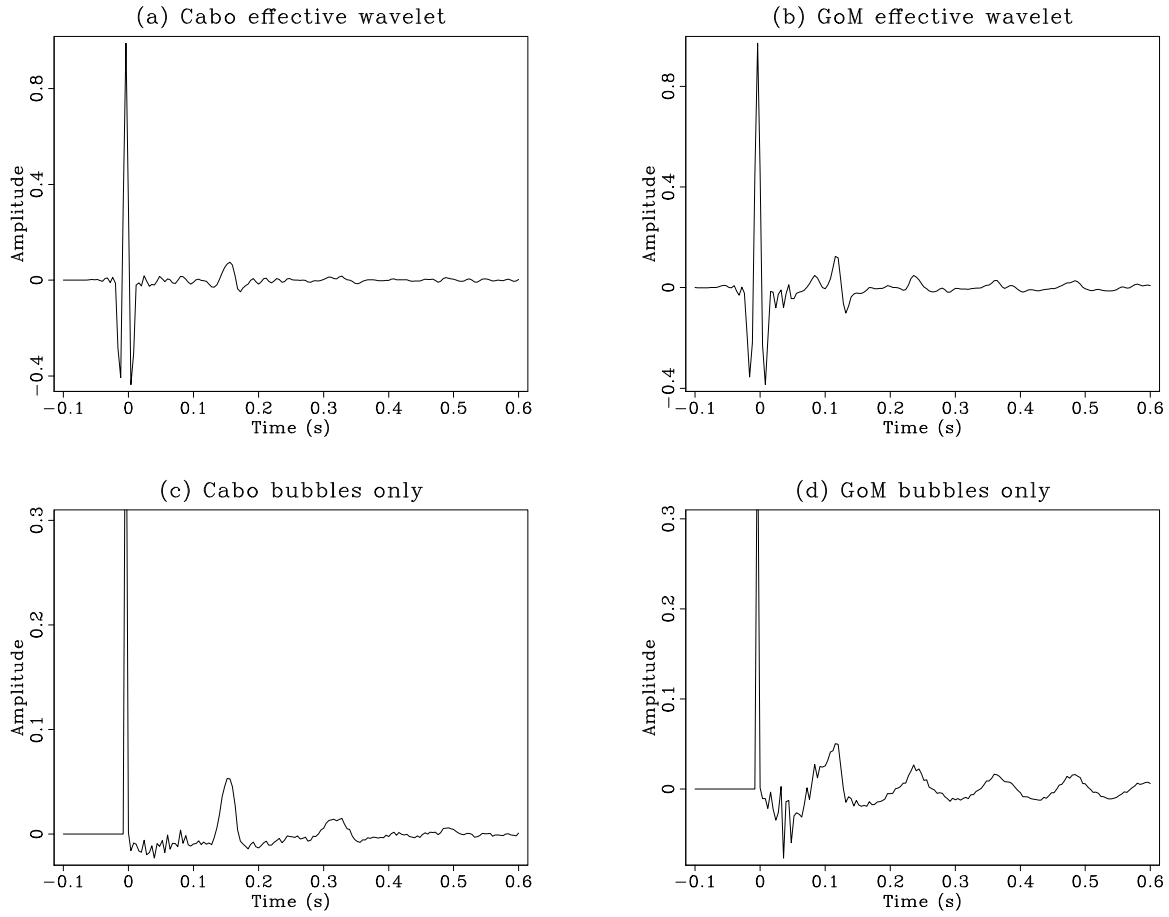


Figure 8: Bottom row shows the seismic source function after the ghosts have been removed (bubble only), top row before. Removing the ghosts reveals the uniform polarity of the bubbles. [**NR**]

Finally, we apply the Ricker deconvolution to a near-offset section from offshore Australia. Figure 9a shows the input data, sampled at 2 ms. Figure 9b shows the deconvolution result (using our default $c = 10$ ms). The Ricker wavelet and bubbles extracted are shown in Figure 10. Note how weak the bubbles are in this case, showing that the gun array was very well tuned (contrary to the other two field data examples, because the bubbles are so small, we decided against showing the debubbled section).

## CONCLUSION

The proposed analytical method, a simple addition to the Kolmogoroff factorization, works well on the three data sets tested. Simply stated, phase, normally a function

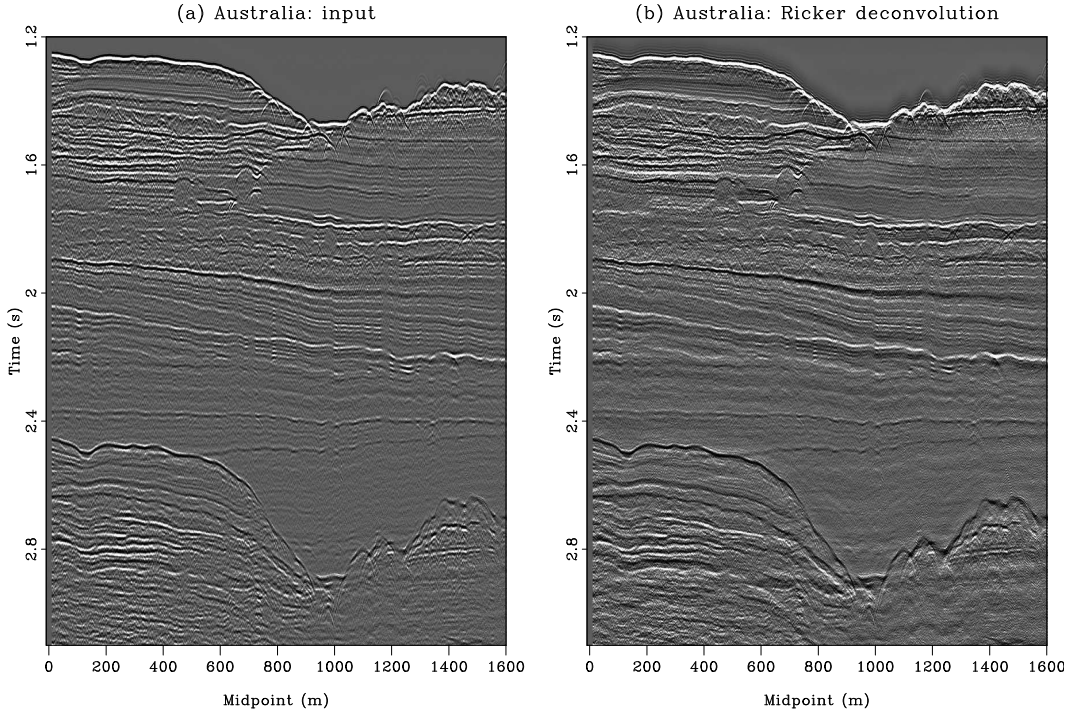


Figure 9: Dataset from offshore Australia (a) before and (b) after Ricker deconvolution. [**NR**]

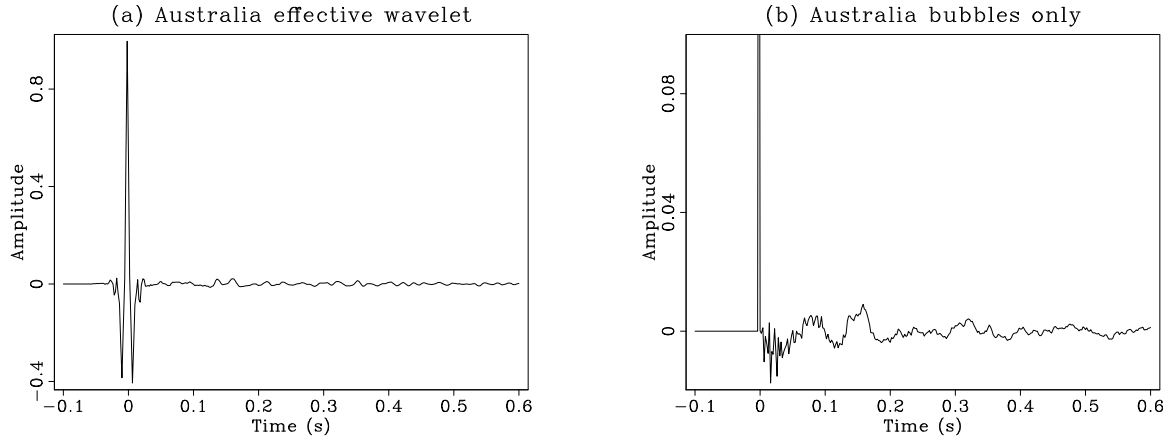


Figure 10: Waveforms extracted from the Australia datasets: (a) effective Ricker wavelet and (b) estimated bubbles. In this case, the bubbles are very weak. [**NR**]

of frequency, is brought into the time lag domain and altered (suppressed) near zero lag. Additionally, it might provide an initialization and provide a regularization that should be helpful in fitting more complicated data models.

## REFERENCES

Ghosh, S., 2000, Deconvolving the ghost effect of the water surface in marine seismics: Geophysics, **65**, 1831–1836.

Jin, D. and J. Rogers, 1983, Homomorphic deconvolution: Geophysics, **48**, 1014–1016.

Levy, S. and D. Oldenburg, 1982, The deconvolution of phase-shifted wavelets: Geophysics, **47**, 1285–1294.

Lindsey, J., 1960, Elimination of seismic ghost reflections by means of a linear filter: Geophysics, **25**, 130–140.

Rice, R., 1962, Inverse convolution filters: Geophysics, **27**, 4–18.

Ricker, N., 1953, The form and laws of propagation of seismic wavelets: Geophysics, **18**, 10–40.

Robinson, E. and S. Treitel, 1964, Principles of digital filtering: Geophysics, **29**, 395–404.

Sacchi, M. and T. Ulrych, 2000, Nonminimum-phase wavelet estimation using higher order statistics: The Leading Edge, **19**, 80–83.

Velis, D., 2008, Stochastic sparse-spike deconvolution: Geophysics, **73**, R1–R9.